



ELSEVIER

Available online at www.sciencedirect.com

SCIENCE @ DIRECT®

**Nonlinear
Analysis**

Real World Applications

Nonlinear Analysis: Real World Applications 6 (2005) 914–934

www.elsevier.com/locate/na

Numerical exploration of a system of reaction–diffusion equations with internal and transient layers

Ana Maria Soane, Matthias K. Gobbert*, Thomas I. Seidman

Department of Mathematics and Statistics, University of Maryland, Baltimore County, 1000 Hilltop Circle, Baltimore, MD 21250, USA

Received 23 November 2004; accepted 29 November 2004

Abstract

A reaction pathway for a classical two-species reaction is considered with one reaction that is several orders of magnitudes faster than the other. To sustain the fast reaction, the transport and reaction effects must balance in such a way as to give an internal layer in space. For the steady-state problem, existing singular perturbation analysis rigorously proves the correct scaling of the internal layer. This work reports the results of exploratory numerical simulations that are designed to provide guidance for the analysis to be performed for the transient problem. The full model is comprised of a system of time-dependent reaction–diffusion equations coupled through the non-linear reaction terms with mixed Dirichlet and Neumann boundary conditions. In addition to internal layers in space, the time-dependent problem possesses an initial transient layer in time. To resolve both types of layers as accurately as possible, we design a finite element method with analytic evaluation of all integrals. This avoids all errors associated with the evaluation of the non-linearities and allows us to provide an analytic Jacobian matrix to the implicit time stepping method. The numerical results show that the method resolves the localized sharp gradients accurately and can predict the scaling of the internal layers for the time-dependent problem.

© 2005 Elsevier Ltd. All rights reserved.

MSC: 35K57; 65M50; 65M60; 76N20

Keywords: Reaction–diffusion equation; Internal layer; Transient layer; Method of lines; Finite element method

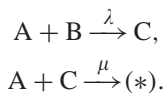
* Corresponding author. Tel.: +1 410 455 2404; fax: +1 410 455 1066.

E-mail addresses: asoane@math.umbc.edu (A.M. Soane), gobbert@math.umbc.edu (M.K. Gobbert), seidman@math.umbc.edu (T.I. Seidman).

1. Introduction

We consider a classical chemical reaction between two species A and B to form a product, generically denoted by (*), according to the reaction mechanism $2A + B \rightarrow (*)$. This reaction takes place within a thin membrane between ‘tanks’ with abundant supplies of A to the left and of B to the right of the membrane. We model the transport inside the membrane as diffusive, thus the model will be given by a system of reaction–diffusion equations that are coupled through the non-linear reaction terms.

This problem is intriguing mathematically, if one considers a more detailed model of the reaction pathway involving an intermediate species C that is generated by a ‘fast’ reaction wherever A and B coexist and depleted comparably ‘slowly’ by reacting with A to form the product



Here, λ , μ are the rate coefficients with the units scaled so that $\lambda \gg \mu = 1$, making the first reaction ‘fast’ relative to the second one. This model implies that wherever A and B coexist the fast reaction depletes them both until only one is left. After this rapid transient period, the continued reaction between A and B relies on diffusion to supply the reactants and will take place only at interface between regions of the two reactants. For the generation of the product to continue at a steady-state, a particular balance between the reactions and diffusion is thus necessary. We intend to attack this problem from both analytic and numerical angles. The rigorous singular perturbation *analysis* for the *steady-state problem* was provided by Seidman and Kalachev [5,11]. This paper presents results of the *numerical* approach for the *time-dependent problem* that allow the exploration of conjectures about the system’s behavior before attempting the rigorous analysis.

The paper is organized as follows: Section 2 details the model, reviews the known results for the stationary problem, and formulates our conjectures for the behavior of the transient problem. Section 3 explains how the numerical method is based on the expectations for the transient problem. Section 4 introduces the simulation results that are presented in detail in Sections 5 and 6. Finally, Section 7 summarizes the conclusions we can draw from the simulations for the behavior of the system.

2. The model

Assuming equal diffusion coefficients for the three species, it is possible to choose units to simultaneously scale the thickness of the membrane, the slower reaction rate, and the diffusion coefficients to 1. The balance of reactions and diffusion over time is then described by the coupled system of non-linear reaction–diffusion equations

$$\left. \begin{aligned} u_t &= u_{xx} - \lambda uv - uw, \\ v_t &= v_{xx} - \lambda uv, \\ w_t &= w_{xx} + \lambda uv - uw \end{aligned} \right\} \text{ in } \Omega = (0, 1), \quad (1)$$

where $u(x, t)$, $v(x, t)$, $w(x, t)$ denote the concentrations of the chemical species A, B, C, respectively. We assume that the species A is supplied with a given fixed concentration $\alpha > 0$ at $x = 0$, and species B with $\beta > 0$ at $x = 1$. No species flows through any other part of the boundary. This results in the mixed Dirichlet and Neumann boundary conditions

$$\begin{aligned} u &= \alpha, & v_x &= 0, & w_x &= 0 & \text{at } x = 0, \\ u_x &= 0, & v &= \beta, & w_x &= 0 & \text{at } x = 1. \end{aligned} \tag{2}$$

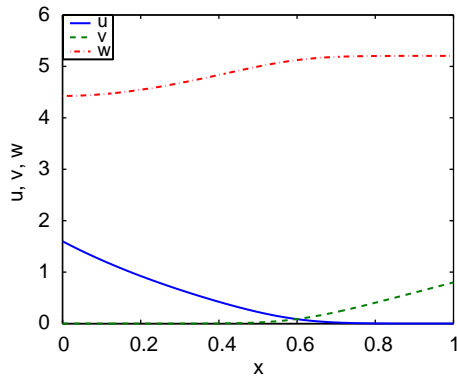
We assume that the non-negative initial concentrations are given

$$u = u_{\text{ini}}(x), \quad v = v_{\text{ini}}(x), \quad w = w_{\text{ini}}(x) \quad \text{at } t = 0. \tag{3}$$

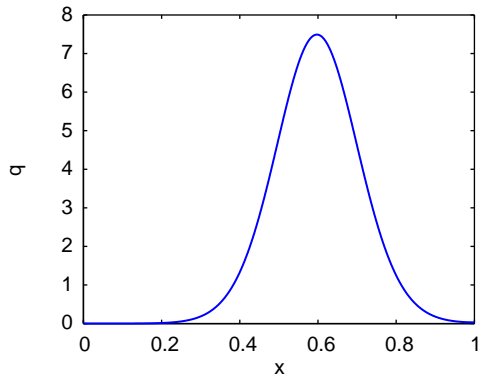
The product is not explicitly tracked in the differential equations. We assume that the boundary and initial data are posed consistently, that is, $u_{\text{ini}}(0) = \alpha$ and $v_{\text{ini}}(1) = \beta$.

Due to the appearance of the large factor $\lambda \gg 1$ in one of the terms in each reaction–diffusion equation in (1), the equations have features of singularly perturbed problems. A standard form for such problems features a small factor as diffusion coefficient in front of the u_{xx} term. For a general introduction to singularly perturbed convection–diffusion and reaction–diffusion problems and their numerical methods, we refer to [9]. A more recent paper [7] presents a coupled system of stationary singularly perturbed reaction–diffusion equations and shows convergence of a finite difference discretization on a non-uniform mesh of Shishkin type for this problem uniformly in the perturbation parameter. Our problem (1) is distinguished from those by its non-standard formulation, in which the spatial and time derivatives are of the same order of magnitude and a reaction-term is large, which results in the appearance of internal layers that move in time. In addition, this problem is ‘more’ singular in the sense that its reduced problem is just the algebraic condition $uv = 0$ [5,11].

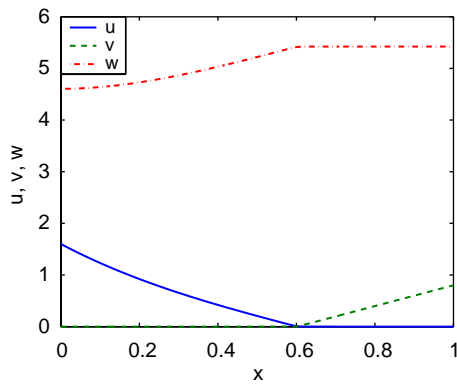
We review now in more detail what is known about the stationary problem given by reaction–diffusion equations (1) accompanied by the boundary conditions (2), but with time-derivatives removed. The existence of a steady-state solution, and the convergence as $\lambda \rightarrow \infty$ to the unique solution of the associated limit problem, was proved in [11]. As a general reference on the analysis techniques, see [15]. In [5], a formal asymptotic expansion of the steady-state solution is constructed, using the methods of singular perturbation theory, and the rate of convergence for the results in [11] is established. In [11], it is also shown that, at steady-state, for each λ large enough there exist some $x^* = x^*(\lambda) \in (0, 1)$ such that $u(x) \geq v(x)$ for $0 \leq x < x^*$ and $u(x) \leq v(x)$ for $x^* < x \leq 1$. At this location x^* , an internal layer occurs in the reaction rate $q := \lambda uv$ of the fast reaction with width $\mathcal{O}(\varepsilon)$ and height $\mathcal{O}(1/\varepsilon)$, where the scaling is given by $\varepsilon = \lambda^{-1/3}$. This behavior is observable in Fig. 1 for simulations with $\alpha = 1.6$ and $\beta = 0.8$. Figs. 1(a), (c), and (e) in the left column show the solution components $u(x)$, $v(x)$, $w(x)$ as functions of x for $\lambda = 10^3$, 10^6 , and 10^9 , respectively. The interface of the region of $u(x) \geq v(x)$ with $u(x) \leq v(x)$ is in this case located at $x^* \approx 0.6$. In the right column, Figs. 1(b), (d), and (f) plot the reaction rate $q(x) = \lambda u(x)v(x)$ of the fast reaction against x for $\lambda = 10^3$, 10^6 , and 10^9 , respectively. At the interface point x^* , the fast reaction rate $q(x)$ has a spike. The numerical results show qualitatively that the width of the spike decreases and its height increases with $\lambda \rightarrow \infty$, as predicted by the theory. To check that the numerical results reproduce the analytically known scaling quantitatively predicted, Fig. 2 plots the scaled rate $\tilde{q}(\zeta) := \varepsilon q(x)$ against



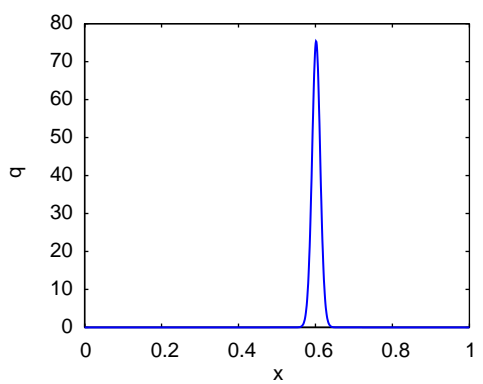
(a) $\lambda = 10^3$



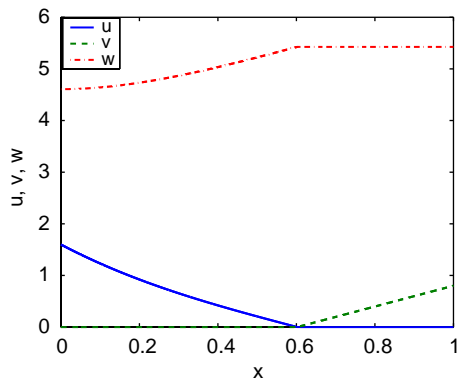
(b) $\lambda = 10^3$



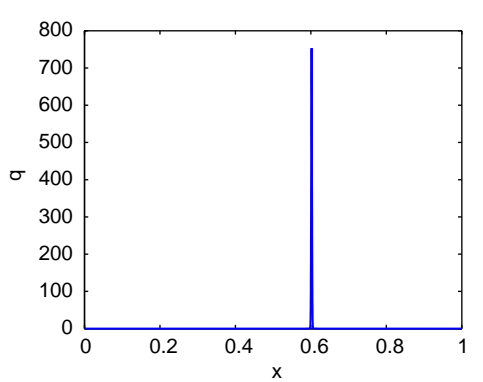
(c) $\lambda = 10^6$



(d) $\lambda = 10^6$



(e) $\lambda = 10^9$



(f) $\lambda = 10^9$

Fig. 1. (a), (c), (e) Solutions of the stationary problem u, v , and w and (b), (d), (f) reaction rate $q = \lambda uv$ for (a) and (b) $\lambda = 10^3$, (c) and (d) $\lambda = 10^6$, and (e) and (f) $\lambda = 10^9$. Notice the different scales of the vertical axes in plots (b), (d), and (f).

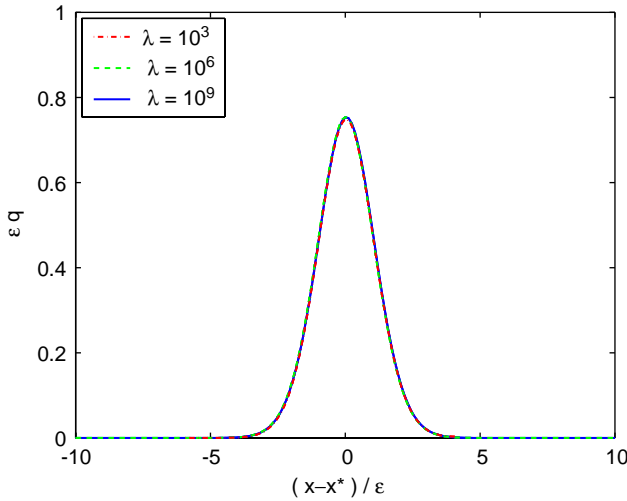


Fig. 2. Plot of the scaled fast reaction rate εq vs. the scaled and shifted position $(x - x^*)/\varepsilon$ for $\lambda = 10^3, 10^6, 10^9$.

the shifted and scaled coordinate $\xi := (x - x^*)/\varepsilon$ with $\varepsilon = \lambda^{-1/3}$. Since the curves for the three values of λ agree very well, the numerical results confirm the scaling obtained analytically in [5].

Using the knowledge about the behavior of the stationary problem, we now formulate some conjectures about the behavior of the time-dependent problem:

- (1) Analogously to the behavior of the system at steady-state, we expect that the solution of the time-dependent system will also exhibit one or more internal layers.
- (2) If the species A and B coexist initially, we expect them to react locally during a rapid transient layer (of duration $\mathcal{O}(1/\lambda)$). After this initial layer, the domain is partitioned into subintervals with either $u \approx 0$ or $v \approx 0$, separated by interfaces.
- (3) During a secondary initial phase (of duration $\mathcal{O}(1)$ with respect to λ), we expect these interfaces to move smoothly and to coalesce (in pairs) over time until only one interface is left. Based on a chemical interpretation of the model, we do not expect that any new interfaces will be created over time.
- (4) Once only one interface is left (or if the initial condition only allowed for one interface), we expect it to move over time to the steady-state position x^* for the value of λ used. That is, we expect the transient solution to converge to the known steady-state solution. The exact motion of the position(s) of the interface(s) over time is not clear at present.

Notice that there are only partial analytical results for the time-dependent problem (1)–(3) available at this point. For instance, existence can be established (for any fixed λ), a lower bound $0 \leq u(x, t), v(x, t), w(x, t)$ can be derived from a maximum principle, and upper bounds independent of λ and t can be established for $u(x, t)$ and $v(x, t)$, though not for $w(x, t)$ (at present). The numerical results are intended to provide significant insight into

the behavior as a guide to analytic studies yet to be performed. For instance, it is of interest to confirm numerically the correct scaling of the internal layers in the transient problem [4].

3. The numerical method

Problem (1)–(3) is a coupled system of non-linear reaction–diffusion equation. It is challenging numerically, because we expect to see both steep gradients in space and rapid transients in time. To discretize the reaction–diffusion equations (1) in space, we use the finite element method with linear basis functions, although reaction–diffusion equations are also often discretized in space by finite difference or finite volume methods [9]. In view of the steady-state results in Fig. 1, we made our choice to try to require as little regularity for the solutions as possible. For linear basis functions, standard finite element theory predicts second-order convergence in the L^2 -norm, provided the mesh resolves the internal layer, i.e., the mesh spacing h satisfies $h < \varepsilon = \lambda^{-1/3}$; at this point, we do not seek a method that is convergent uniformly in λ . The choice of linear basis functions, as opposed to higher-order, more complicated elements, was made to ease the analytic computation of all terms and their Jacobian for the ODE solver; see below.

For simplicity, a uniform mesh is used. We accept at this point that a very fine mesh will be necessary to capture the behavior of the system inside the internal layer(s) for large values of λ . However, this has the advantage that we can capture the layer(s) with the same accuracy, no matter where each might be located at a certain point in time. Given this advantage of simplicity and reliability, a uniform mesh is appropriate. The necessary fine resolution can be easily achieved on computers available today for all λ values of interest. For instance, for $\lambda = 10^9$, we anticipate the interface to have width of order $\varepsilon = \lambda^{-1/3} = 10^{-3}$. Using the rule of thumb that we wish to place at least 8 points inside this layer, we need about 8000 points to cover Ω .

Using the method of lines, we reduce our system to an ODE system in time. To solve this stiff system, we use the `ode15s` solver [12] in MATLAB [8] with automatic step-size and order control, that is suitable to capture the initial transient layer both accurately and efficiently. The finite element discretization involves integrals of the non-linear reaction terms on the right-hand side of (1). Usually, these integrals would require a numerical approximation. Instead, we take advantage of the special form of the non-linearity and obtain the integrals analytically. Besides avoiding potential error from the quadrature, knowing all terms analytically allows us to supply an analytic Jacobian to the ODE method for best accuracy and best efficiency of its integrated non-linear solver, a simplified Newton method. In summary, the method is both accurate and leverages readily available software effectively, solving problem (1)–(3) in fewer than 250 lines of MATLAB code. For additional details on the numerical method as well as extensive numerical convergence and performance studies, see [13].

Another option would have been to apply the parabolic solver in a commercial software package such as FEMLAB 2.3 [2] directly to problem (1)–(3). We chose, however, to develop the finite element discretization ourselves, for the following reasons.

In fact, one reason for the choice of the finite element method was the ability to check the solution against this established software package. Therefore, we restrict our code to

a standard finite element formulation and to MATLAB's `ode15s`, equivalent to available components in FEMLAB 2.3, so we are able to check our code against FEMLAB. We find that, for instance, the number of time steps taken are equal, giving confidence that the codes give equivalent solutions; for these results and a convergence study for the finite element discretization, see [13].

One downside resulting from following FEMLAB's approach is that neither it nor our method can guarantee the non-negativity of solutions. We have tracked the minimum value of the numerical solutions and have observed small negative values of the same magnitude for both codes for large values of λ . Computationally, tests with a decreasing tolerance of the ODE method lead to decreasing magnitudes of negative values, hence we are able to control those numbers. Analytically, we know that our spatial discretization with a lumped mass matrix together with the implicit Euler method in time does guarantee the non-negativity of the solution [3,10]. But it turns out that even when restricting MATLAB's `ode15s` to the implicit Euler method, small negative values in the solution persist. This is the result of the non-linear solver, a simplified Newton method, inside `ode15s` that is not especially designed to preserve non-negativity; this behavior agrees with the prediction in [10]. We note also that restricting `ode15s` to method order $k = 1$ is costly computationally. Since even this cannot guarantee non-negativity, we stick with the higher efficiency of a variable order method, in agreement with FEMLAB, for now, in order to retain the ability to compare our method directly to FEMLAB. This is an interesting line of research for the future, for which we will be able to take advantage of our own code and design a different formulation that guarantees the non-negativity of the solution.

Additionally, for problems such as these with internal layers with rapidly varying quantities, it would clearly be desirable to use adaptive mesh refinement and coarsening so as to use a fine mesh exactly in those regions of Ω around the internal layers. For instance, singularly perturbed stationary convection–diffusion equation in standard form are considered in [6,14], that propose moving mesh algorithms (with fixed number of nodes) and present rigorous convergence analyses and numerical examples of the methods uniformly in the perturbation parameter. An adaptive method for a time-dependent heat equation in one spatial dimension is presented, for instance, in [1]. The results in these references cannot be applied directly to our problem, as it is posed in a different, non-standard form. (Notice that due to the unknown and moving location of the internal layers, it is not possible to design a specialized, but fixed in time, mesh of Shishkin type a priori.) For the *stationary* problem, the results in Fig. 1 were checked against FEMLAB 2.3 with adaptivity; the adaptive method demonstrated its effectiveness by using more than an order of magnitude fewer nodes than the uniform mesh. But FEMLAB 2.3 does not have an adaptive solver for the time-dependent problems at present, so this was not an option available at this time.

Hence, this work uses a uniform over-discretization of the domain and does not propose a method that converges uniformly in λ . The results on this over-resolved mesh will be useful in the future to assess the accuracy of alternative, in particular, adaptive methods. The desire to generalize our code to non-uniform meshes in the future is another reason for our insistence on hand coding the spatial discretization for our numerical method. Moreover, higher-dimensional formulations of problem (1)–(3) are of interest in applications, and our code will control the use of memory better than a black-box package. For instance, our

numerical tests show that our implementation is about a factor 3 faster and to use 40% less memory than FEMLAB 2.3 [13].

4. Simulation results

The following two sections reports the details of the numerical results for the time-dependent problem (1)–(3). In all cases, we use the values $\alpha = 1.6$ and $\beta = 0.8$, and compute over the time interval $0 \leq t \leq 10$. This final time for the time-dependent simulations proves sufficient to approximate steady-state. Section 5 reports detailed results of various computed quantities for the value of $\lambda = 10^6$. This value is chosen because, based on the steady-state results, we expect internal layers with width on the order of $\varepsilon = \lambda^{-1/3} = 0.01$ and this width is still large enough to be discernible in plots on the scale of the domain $\Omega = (0, 1)$. For this fixed value of λ , three different types of initial conditions of increasing complexity are considered. Section 6 combines results for three different values of $\lambda = 10^3, 10^6, 10^9$ to analyze the behavior as $\lambda \rightarrow \infty$. To this end, the crucial quantity $q = \lambda uv$ is considered.

In each case, the number of nodes N of the uniform numerical mesh is chosen to guarantee at least 8 mesh points within the width of the internal layers, anticipated as $\varepsilon = \lambda^{-1/3}$. That is, we use (at least) $N = 129$ for $\lambda = 10^3$, $N = 1025$ for $\lambda = 10^6$ and $N = 8193$ for $\lambda = 10^9$. Notice that N is chosen so that the mesh size $h = 1/(N - 1)$ is a computer number to avoid unnecessary round-off in calculations with h . The choice of time step Δt and method order k of the NDFk method is performed automatically by MATLAB's `ode15s` function [8,12]. We control the accuracy of the method by selecting relative and absolute tolerances on the estimated truncation error of the ODE method; we typically used tolerances similar to MATLAB's default choice, say, `RelTol` = 10^{-3} , `AbsTol` = 10^{-6} . In fact, simulations were performed for a range of values for N (up to 16,385) and the ODE tolerances (down to 10^{-14}) and also some simulations compared to results from FEMLAB 2.3 [2]. Therefore, we feel comfortable that the simulation results are reliable.

The following two sections collect the detailed results of the simulations. Section 5 considers three types of initial conditions with increasing degree of complexity for the case of $\lambda = 10^6$ that give rise to internal and transient layers. In order to study the effect of the limit $\lambda \rightarrow \infty$, Section 6 combines the results for all values of λ studied at a fixed time and illustrates the correct scaling of the internal layer.

5. Time-dependent studies for fixed $\lambda = 10^6$

The simulations for the time-dependent problem with $\lambda = 10^6$ were performed for three types of initial conditions of increasing complexity. In all cases, the functions u_{ini} , v_{ini} , and w_{ini} are chosen to satisfy the boundary conditions. Also, since we are interested in internal layers at present, $u_{\text{ini}}(1)$ and $v_{\text{ini}}(0)$ are chosen zero to avoid additional transient layers near the boundary in the approach to steady-state. For all three types of initial conditions we assume that the species C is not present in the domain initially, i.e., we choose $w_{\text{ini}} \equiv 0$.

5.1. Type 1 initial condition: two non-overlapping regions

The simplest type of initial condition is inspired by the steady-state results in Fig. 1, in which the species A and B do not coexist at steady-state, i.e., they occupy non-overlapping geometric regions and with only a single interface. So, we choose also an initial condition comprised of two non-overlapping regions with either $u > 0$ and $v = 0$ or $u = 0$ and $v > 0$. However, we purposefully locate the interface between the two regions at $x = 0.5$, which is significantly different from the steady-state interface at about 0.6. Hence, we expect this interface to move to the right over time. Specifically, we choose

$$\begin{aligned}
 u_{\text{ini}}(x) &= \begin{cases} 6.4(x - 0.5)^2 & \text{if } 0 \leq x < 0.5, \\ 0 & \text{if } 0.5 \leq x \leq 1, \end{cases} \\
 v_{\text{ini}}(x) &= \begin{cases} 0 & \text{if } 0 \leq x < 0.5, \\ 1.6x(x - 0.5) & \text{if } 0.5 \leq x \leq 1, \end{cases} \\
 w_{\text{ini}}(x) &= 0,
 \end{aligned}$$

which is plotted in Fig. 3(a). Since the regions of non-zero concentrations for u and v are chosen non-overlapping, we have $q = \lambda uv \equiv 0$ at $t = 0$, which is confirmed in Fig. 4(a).

Fig. 3 shows the solutions u , v , and w at six different time steps, while Fig. 4 shows the reaction rate $q = \lambda uv$ at the same time steps. After $t = 0$, species A diffuses to the region occupied by B and vice versa. Once the species A and B coexist in the same region, they react rapidly and form C. This behavior can be observed in Fig. 3(b), where we notice an increase in the concentration of C, $w(x)$, around the point 0.5. At the same location, we note the appearance of an internal layer in the reaction rate q , as shown in Fig. 4(b). The width of the layer appears already comparable to the one in the steady-state result in Fig. 1(d), but its height still grows over time to reach the steady-state value. (Notice the different scales on the vertical axes in Figs. 4 and 1(d).) As t increases, C continues to be produced in the region where A and B coexist and the internal layer in the reaction rate q moves to the right. Meanwhile, in the rest of the domain, the concentration of C increases due to diffusion. We can see in Fig. 3(c) that by $t = 0.052$, we have $w(x) > 0$ everywhere in the domain. By $t = 1.053$, the concentration profiles of A and B are close to those at steady-state and at $t = 10$ the steady-state is reached, as can be observed in Figs. 3(e) and (f). Notice in Fig. 4(e) at time $t = 1.053$ that the location of the interface is clearly to the right of the eventual steady-state value.

To visualize the motion of the interface between regions dominated by species A or B for all times $0 \leq t \leq 10$, Fig. 5(a) plots the interface over the entire (x, t) -plane. This plot is determined numerically by computing $z(x, t) := u(x, t) - v(x, t)$ and determining the contour level $z = 0$ using MATLAB's `contour` function. With t increasing on the vertical axis, Fig. 5(a) shows the motion of the interface from $x = 0.5$ at $t = 0$ to a maximum value of about $x \approx 0.65$ at $t \approx 0.5$, before converging more slowly to the steady-state value of about 0.6. Fig. 5(b) zooms in on the transient behavior for $0 \leq t \leq 0.1$.

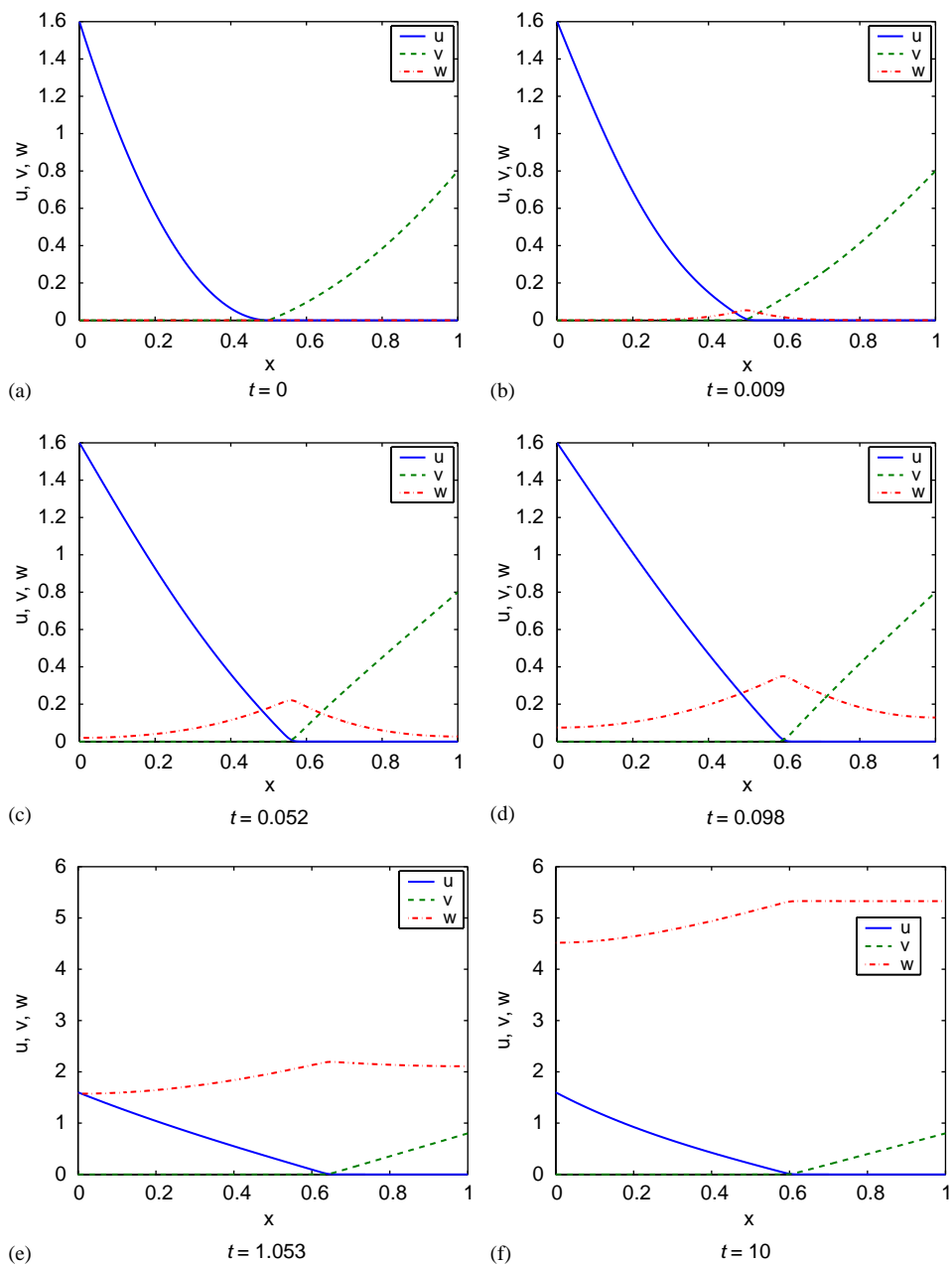


Fig. 3. Plot of the solutions u, v , and w for type 1 initial conditions and $\lambda = 10^6$ at different time steps: (a) $t = 0$, (b) $t = 0.009$, (c) $t = 0.052$, (d) $t = 0.098$, (e) $t = 1.053$, (f) $t = 10$. Notice the different scales on the vertical axes.

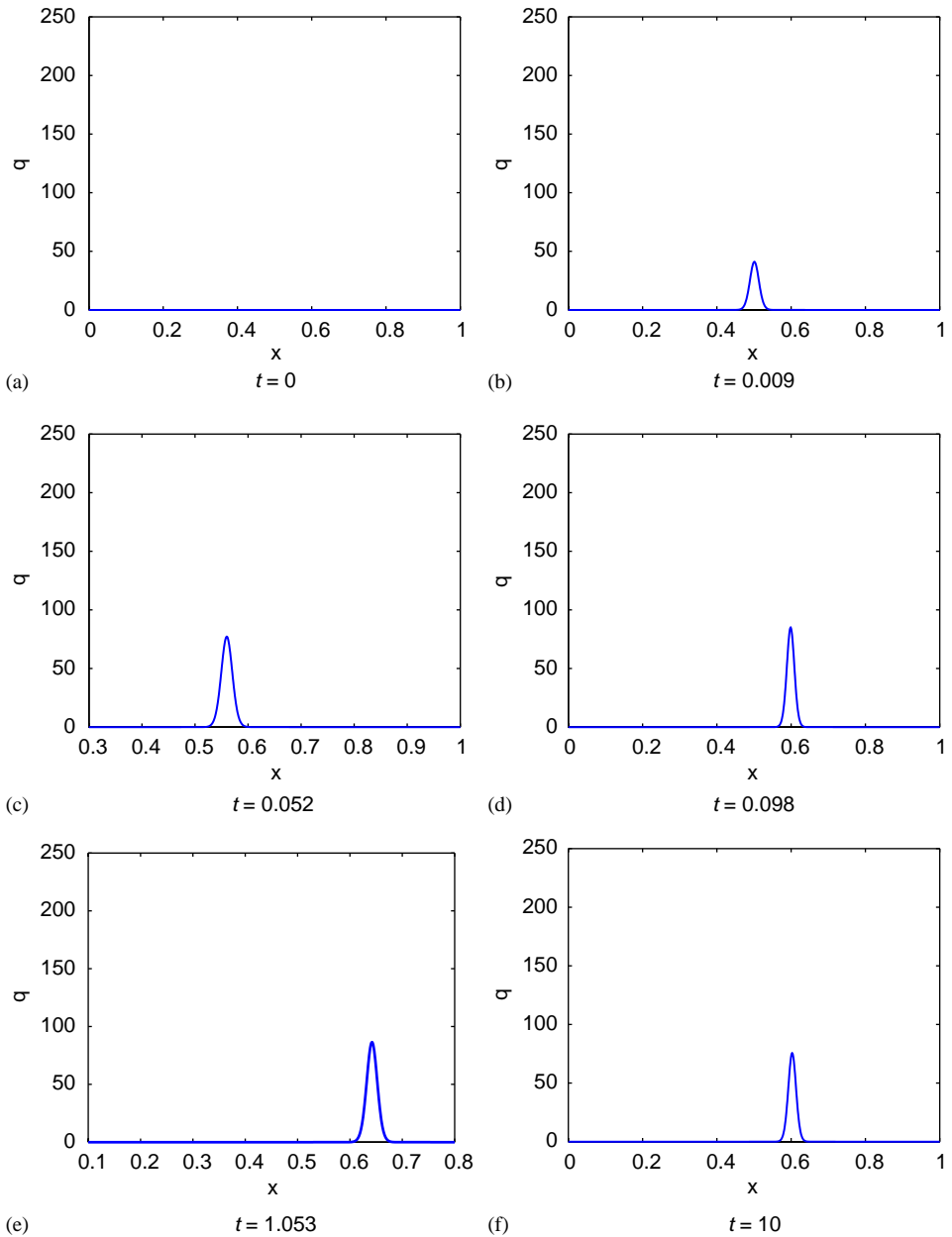


Fig. 4. Plot of the reaction rate $q = \lambda uv$ for type 1 initial condition and $\lambda = 10^6$ at different time steps: (a) $t = 0$, (b) $t = 0.009$, (c) $t = 0.052$, (d) $t = 0.098$, (e) $t = 1.053$, (f) $t = 10$.

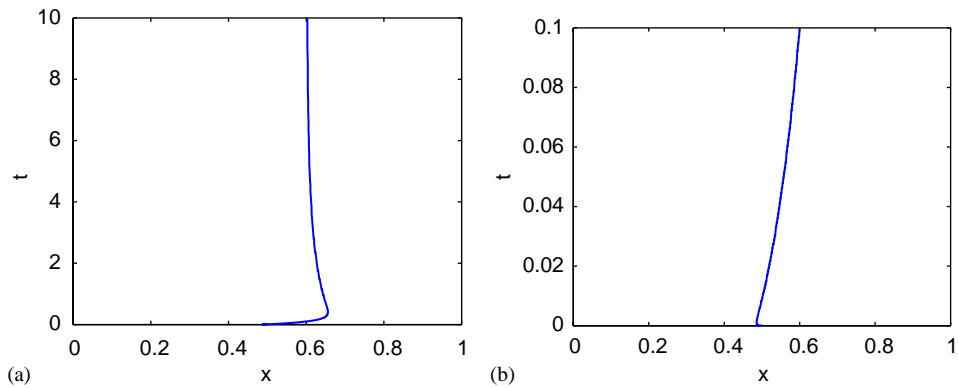


Fig. 5. Motion of internal layer for type 1 initial conditions and $\lambda = 10^6$ for times (a) $0 \leq t \leq 10$ and (b) $0 \leq t \leq 0.1$.

5.2. Type 2 initial condition: four non-overlapping regions

The second type of initial condition is designed so that there will be four non-overlapping regions of species concentrations with either A or B, i.e., we prescribe either $u = 0$ or $v = 0$ at every point in the domain at $t = 0$. Due to diffusion, A and B will contact each other, and the reaction rate $q = \lambda uv$ will become non-zero at the three interfaces between the regions. Since the steady-state solution only admits one interface, we expect two of the three interfaces to coalesce within some initial phase. Concretely, we choose the initial condition

$$\begin{aligned}
 u_{\text{ini}}(x) &= \begin{cases} 6.4(0.25 - x) & \text{if } 0 \leq x < 0.25, \\ 0 & \text{if } 0.25 \leq x < 0.5, \\ 16(0.75 - x)(x - 1) & \text{if } 0.5 \leq x < 0.75, \\ 0 & \text{if } 0.75 \leq x \leq 1, \end{cases} \\
 v_{\text{ini}}(x) &= \begin{cases} 0 & \text{if } 0 \leq x < 0.25, \\ 16(1 - x)(x - 0.25) & \text{if } 0.25 \leq x < 0.5, \\ 0 & \text{if } 0.5 \leq x < 0.75, \\ 3.2(x - 0.75) & \text{if } 0.75 \leq x \leq 1, \end{cases} \\
 w_{\text{ini}}(x) &= 0.
 \end{aligned}$$

This condition is plotted in Fig. 6(a), and the plot of q in Fig. 7(a) confirms that $q = \lambda uv \equiv 0$ initially.

Fig. 6 shows the solutions u , v , and w at six different time steps and Fig. 7 plots the fast reaction rate $q = \lambda uv$ at the same time steps. We observe the rapid appearance of three interfaces when the reaction between species A and B starts. These layers appear to have comparable width to the one in the steady-state result in Fig. 1(d). (Notice the different scales on the vertical axes in Figs. 7 and 1(d).) The layers move and within quite a short period of time, two of the layers coalesce; indeed, by time $t = 0.021$ there is only one internal layer, as can be seen in Fig. 7(d). By $t = 1.228$ in Fig. 7(e), also its height has reached the steady-state value, while it continues to move to the steady-state location at about 0.6, which is reached by $t = 10$ in Fig. 7(f).

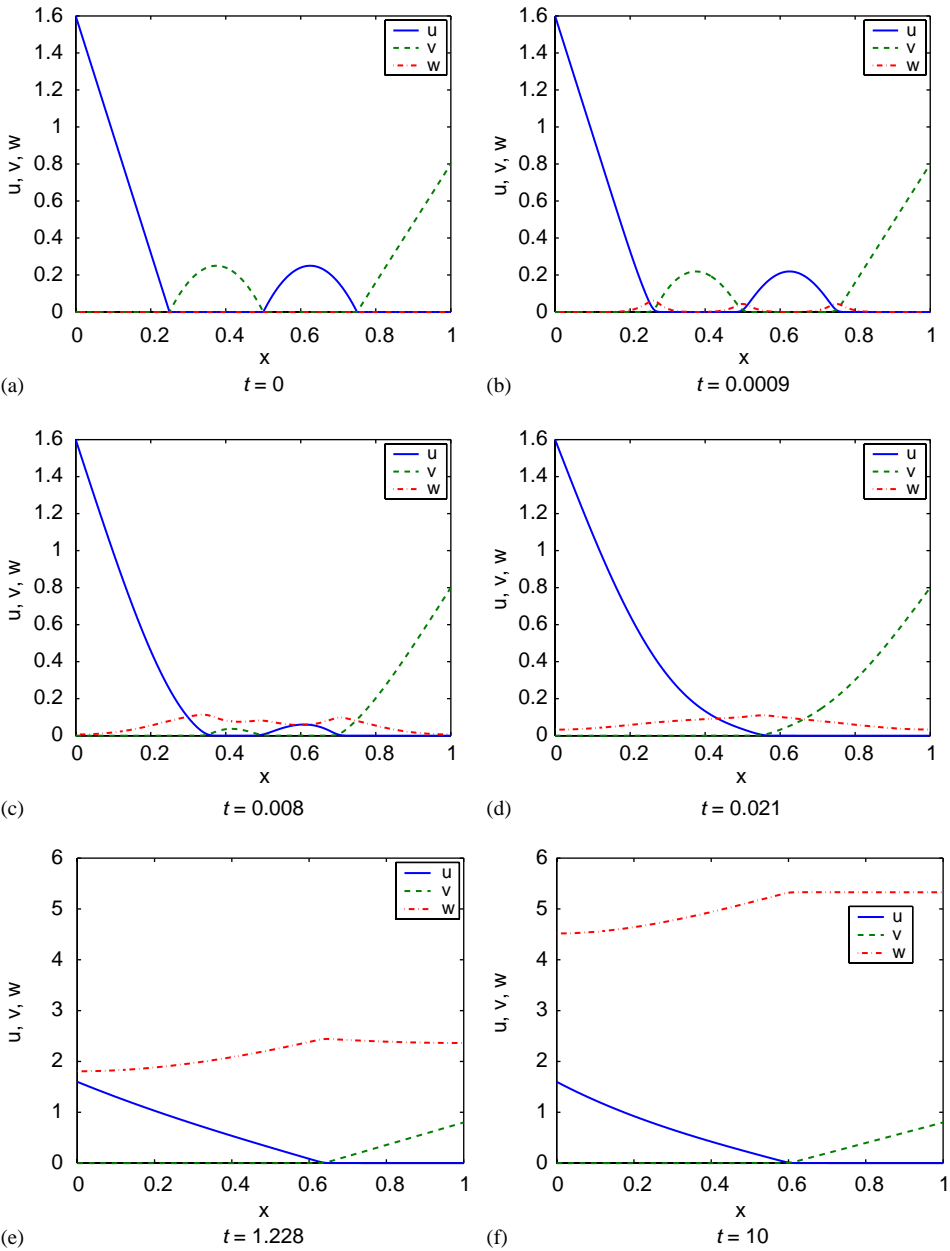


Fig. 6. Plot of the solutions u, v , and w for type 2 initial conditions and $\lambda = 10^6$ at different time steps: (a) $t = 0$, (b) $t = 0.0009$, (c) $t = 0.008$, (d) $t = 0.021$, (e) $t = 1.228$, (f) $t = 10$. Notice the different scales on the vertical axes.

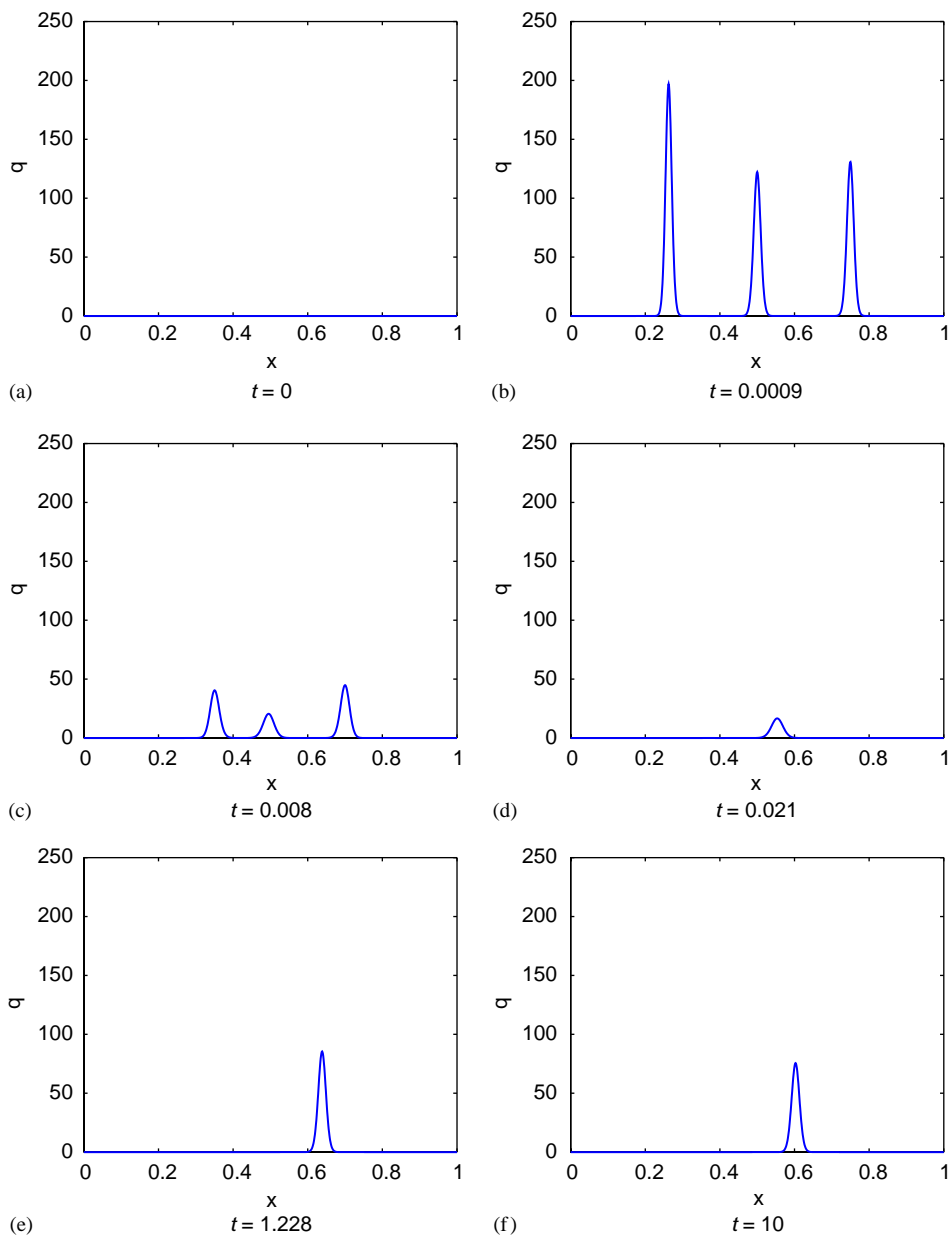


Fig. 7. Plot of the reaction rate $q = \lambda uv$ for type 2 initial condition and $\lambda = 10^6$ at different time steps: (a) $t = 0$, (b) $t = 0.0009$, (c) $t = 0.008$, (d) $t = 0.021$, (e) $t = 1.228$, (f) $t = 10$.

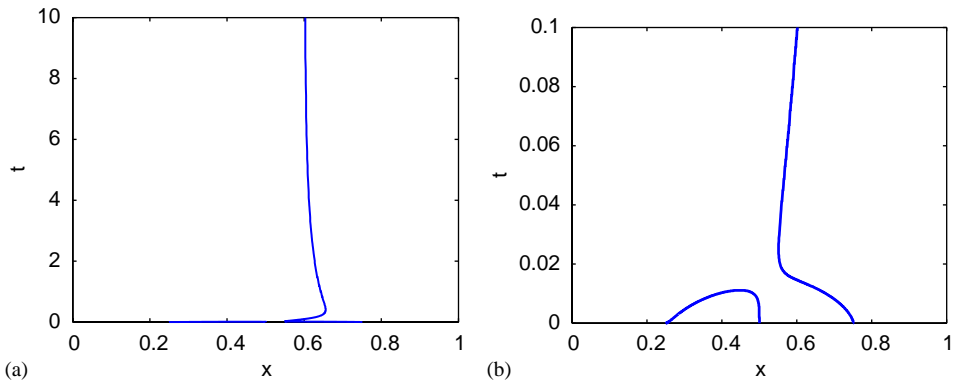


Fig. 8. Motion of internal layers for type 2 initial conditions and $\lambda = 10^6$ for times (a) $0 \leq t \leq 10$ and (b) $0 \leq t \leq 0.1$.

We again analyze the interface motion in detail. Fig. 8(a) plots the interface over the entire (x, t) -plane for all $0 \leq t \leq 10$. We notice again that the sole remaining interface after the initial transient moves to the right, before approaching the steady-state value from the right. To see the coalescing behavior more clearly, Fig. 8(b) zooms in on the time interval $0 \leq t \leq 0.1$. We notice that by time $t \approx 0.01$, the first and second interface have coalesced. It is interesting to notice in Fig. 8(b) that the third interface originally moved to the left towards the other interfaces, before moving to the right, as seen in Fig. 8(a).

5.3. Type 3 initial condition: four overlapping regions

The third type of initial condition implements a more general case in which the species A and B are allowed to coexist everywhere in the domain initially: their regions overlap. We design it so that there are alternately two regions with $u > v$ and two regions with $u < v$; we anticipate that this should result in three interfaces developing. More precisely, we conjecture that there will be two initial transient behaviors: Due to the fast nature of the reaction between A and B, we expect that diffusion and the slower reaction will be comparatively negligible: the intermediate C will be created extremely rapidly initially, until either A or B is depleted at each point in the domain. At this time, there will be three interfaces between the four non-overlapping regions solely occupied by A or B. During a second, slower phase, two of the three interfaces should coalesce and the remaining one tend to the steady-state value, just as in the previous case. Specifically, we choose

$$\begin{aligned}
 u_{\text{ini}}(x) &= 27.3x^4 - 67x^3 + 53.7x^2 - 15.6x + 1.6, \\
 v_{\text{ini}}(x) &= 9x^4 - 13.77x^3 + 5.57x^2, \\
 w_{\text{ini}}(x) &= 0.
 \end{aligned}$$

This is plotted in Fig. 9(a). Notice that $u > v$ for about $0 \leq x \leq 0.2$ and $0.35 \leq x \leq 0.85$, with $u < v$ in the remaining regions. At the initial time $t = 0$, the reaction rate $q = \lambda uv$ is positive (and large), in contrast to the other two types of initial conditions; this is confirmed by Fig. 10(a).

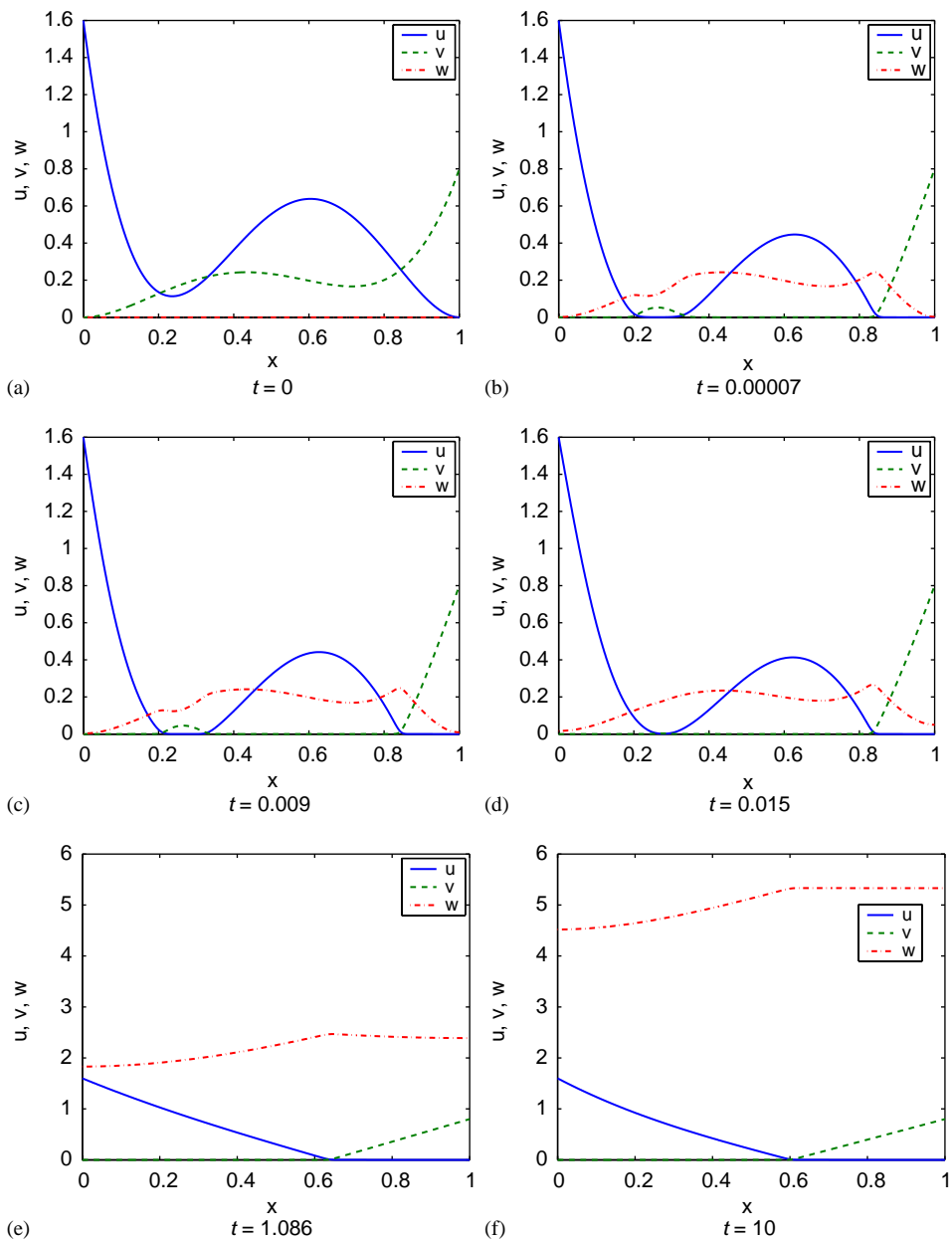


Fig. 9. Plot of the solutions u, v , and w for type 3 initial conditions and $\lambda = 10^6$ at different time steps: (a) $t = 0$, (b) $t = 0.00007$, (c) $t = 0.009$, (d) $t = 0.015$, (e) $t = 1.086$, (f) $t = 10$. Notice the different scales on the vertical axes.

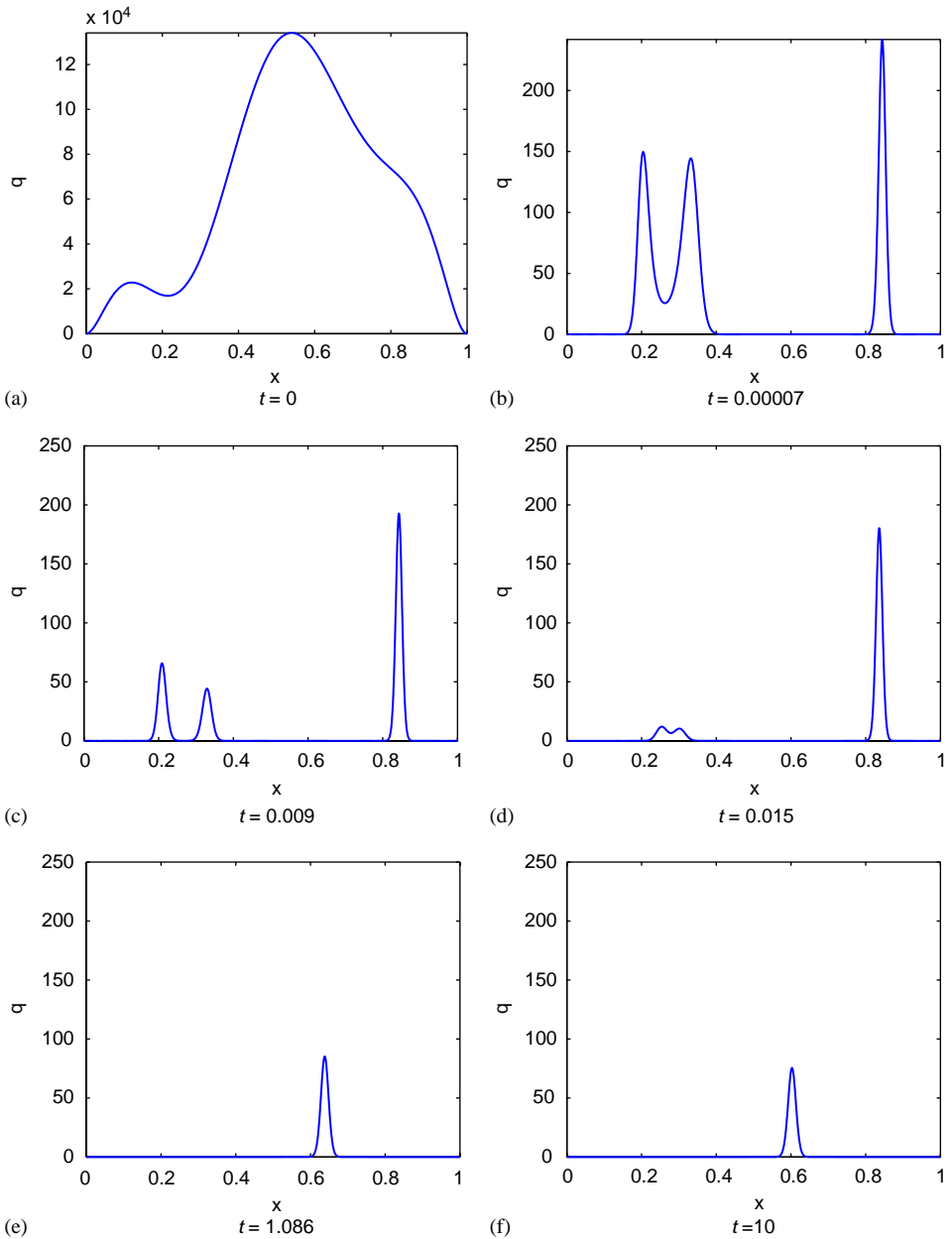


Fig. 10. Plot of the reaction rate $q = \lambda uv$ for type 3 initial condition and $\lambda = 10^6$ at different time steps: (a) $t = 0$, (b) $t = 0.00007$, (c) $t = 0.009$, (d) $t = 0.015$, (e) $t = 1.086$, (f) $t = 10$. Notice the different scales on the vertical axes.

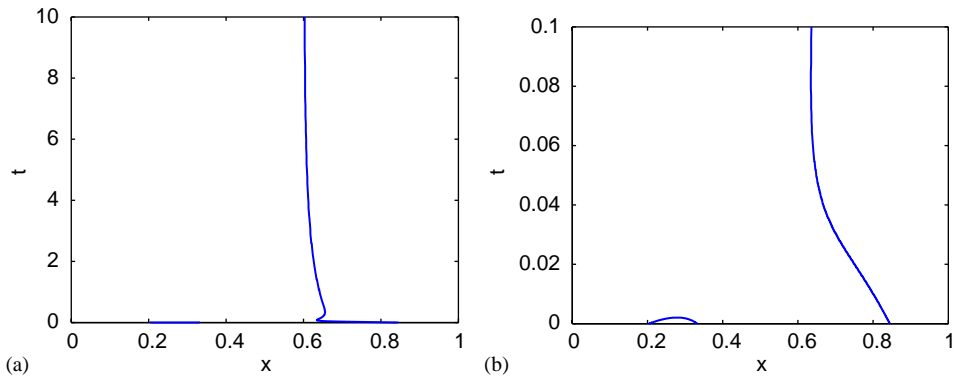


Fig. 11. Motion of internal layers for type 3 initial conditions and $\lambda=10^6$ for times (a) $0 \leq t \leq 10$ and (b) $0 \leq t \leq 0.1$.

Fig. 9 shows the solutions $u, v,$ and w at six different time steps. Fig. 10 plots the reaction rate $q = \lambda uv$ at the corresponding time steps. We notice the change in magnitude of the reaction rate in the very short time interval $0 \leq t \leq 0.00007$. Also, once the species A and B start reacting, three internal layers all of roughly the same width occur in the reaction rate q , see Fig. 10(c) at $t = 0.009$. Two of these layers coalesce and the third one moves to the steady-state location by $t = 10$. Again, the layers attain the *width* of the steady-state layer in Fig. 1(d) very quickly, while their *height* continues to adjust over time. (Notice the different scales on the vertical axes in Figs. 10 and 1(d).)

Fig. 11(a) shows the motion of the interfaces in the (x, t) -plane for $0 \leq t \leq 10$. The overall behavior is similar to, but faster than the previous case. We see in the zoom in Fig. 11(b) for $0 \leq t \leq 0.1$ that the first two interfaces coalesce by $t < 0.05$, which is indeed faster than observed in Fig. 8(b).

6. Asymptotic results for $\lambda \rightarrow \infty$

Recall that one major purpose of the numerical simulations was to provide guidance as to the asymptotic behavior of the solutions as $\lambda \rightarrow \infty$. To this end, we conduct studies for the three progressively larger values of $\lambda = 10^3, 10^6, 10^9$. Similar qualitative results were obtained as presented for $\lambda = 10^6$ in the previous section; the cases were distinguished by the width and height of $q = \lambda uv$ of each interface: the width decreased and the height increased with growing λ . We conjecture that the scaling is the same as has been proven analytically for the steady-state, namely as $\varepsilon = \lambda^{-1/3}$; no such analytic results are presently available for the time-dependent problem (1)–(3). To check the conjecture, we pick a time after the initial transient phase such that only one internal layer exists and scale the reaction rate q . Fig. 12 shows this scaled quantity $\tilde{q} = \varepsilon q$ plotted vs. the scaled and shifted variable $\xi = (x - x^*)/\varepsilon$, where x^* is the numerically determined location of the interface at this time. Fig. 12(a), (b), and (c) show the plots for the type 1, type 2, and type 3 initial conditions, respectively. Fig. 12 is at $t = 1$, but similar results were already observed for, e.g., $t = 0.1$. Notice that the convergence with $\lambda \rightarrow \infty$ is rather quick, as the scaled rates for all values

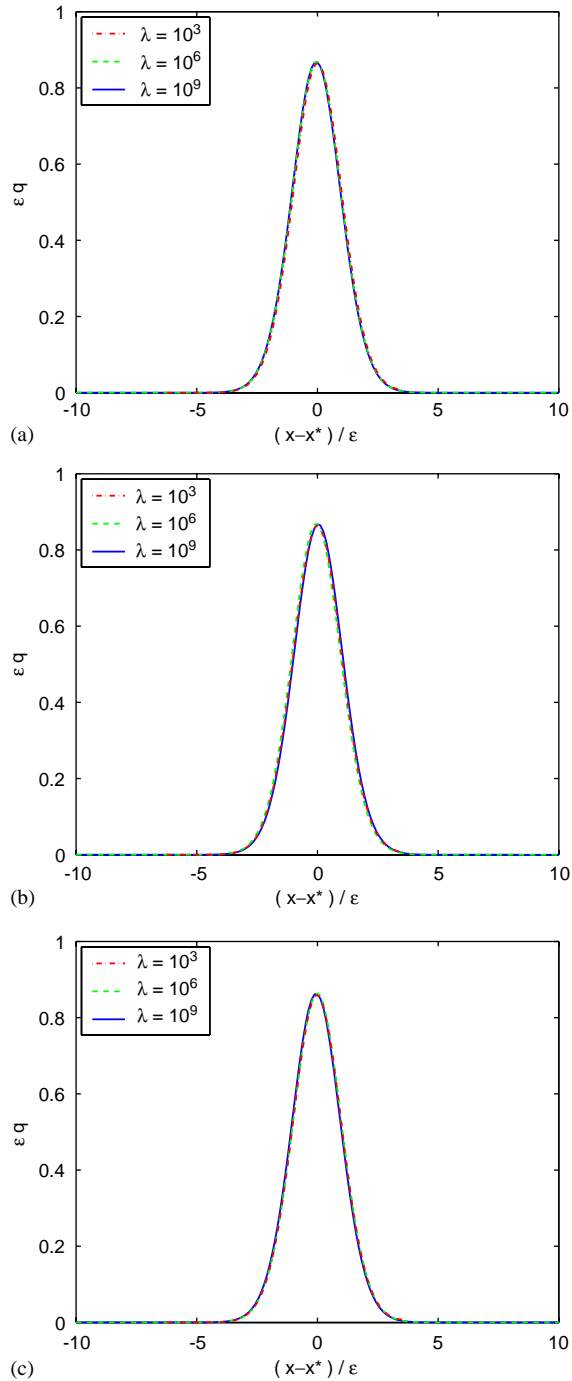


Fig. 12. Plot of the scaled fast reaction rate ϵq vs. the scaled and shifted position $(x - x^*)/\epsilon$ at time $t = 1$ for $\lambda = 10^3, 10^6, 10^9$, for (a) type 1 initial conditions, (b) type 2 initial conditions, and (c) type 3 initial conditions.

of λ agree with each other very well. This confirms the expected scaling $\varepsilon = \lambda^{-1/3}$ for the internal layers.

7. Conclusions

The simulations in the previous two sections allow us to draw the following conclusions about the behavior of the solutions to problem (1)–(3):

- Section 5 considered three types of initial conditions with increasing degree of complexity for the case of $\lambda = 10^6$. If species A and B coexist initially at a point in the domain, the fast reaction depletes both reactants in a rapid initial transient layer, until only one of the species remains at this point. This confirms the conjecture about the smooth behavior of the interfaces and their monotone coalescence. If the initial condition had several, say, four regions where alternately $u > v$ and $u < v$, then three interfaces between regions with $v \approx 0$ and $u \approx 0$ develop during this transition. The fast reaction rate $q = \lambda uv$ is zero wherever either $u \approx 0$ or $v \approx 0$ and has large values inside the interfaces, where non-vanishing concentrations of A and B meet. Outside of this initial transient layer, the *width* of the internal layers is on the same order of magnitude as at steady-state. In a second phase of the system evolution, all but one of the interfaces coalesce in pairs. After this phase, the remaining interface has already the same *width* and *height* of the interface at steady-state, but still moves over time to its steady-state location. The results validate that the transient solution tends to the steady-state. We note that this result is not obvious as no proof exists for the fact that $w(x, t)$ stays bounded over time. One additional—and unexpected—observation is that the remaining interface, after all but one have coalesced, might overshoot the location of the steady-state interface initially.
- When combining in Section 6 the results for all values of λ studied, we can confirm that after the coalescing phase the remaining internal layer has the *width* $\mathcal{O}(\varepsilon)$ and *height* $\mathcal{O}(1/\varepsilon)$ with the same scaling $\varepsilon = \lambda^{-1/3}$ as the steady-state problem. This result has not yet been shown analytically.

In this paper, we have not analyzed the durations of the initial transient and coalescence phases, yet. Neither have simulations for additional initial conditions or for different values of α and β been performed that might lead to different motions of the interfaces. However, we believe that the results presented here are typical and show all qualitative features to be expected. Since they were obtained on an over-refined, fixed mesh and the numerical method compared to an established finite element package, the results are reliable and form a solid basis for designing more efficient numerical methods, for instance, based on adaptive mesh refinement and coarsening.

Acknowledgements

We gratefully acknowledge the financial support from the University of Maryland, Baltimore County through a summer faculty fellowship and research assistant support. The

second author also wishes to thank the Institute for Mathematics and its Applications (IMA) at the University of Minnesota for its hospitality during Fall 2004. The IMA is supported by funds provided by the U.S. National Science Foundation. Furthermore, we would like to thank L.V. Kalachev, M. Stynes, and C. Xenophontos for useful comments and discussions.

References

- [1] J.M. Coyle, J.E. Flaherty, R. Ludwig, On the stability of mesh equidistribution strategies for time-dependent partial differential equations, *J. Comput. Phys.* 62 (1986) 26–39.
- [2] FEMLAB Version 2.3, COMSOL AB, www.comsol.com.
- [3] W. Hundsdorfer, J. Verwer, *Numerical Solution of Time-Dependent Advection–Diffusion–Reaction Equations*, Springer Series in Computational Mathematics, vol. 33, Springer, Berlin, 2003.
- [4] L.V. Kalachev, Personal communication.
- [5] L.V. Kalachev, T.I. Seidman, Singular perturbation analysis of a stationary diffusion/reaction system whose solution exhibits a corner-type behavior in the interior of the domain, *J. Math. Anal. Appl.* 288 (2003) 722–743.
- [6] N. Kopteva, M. Stynes, A robust adaptive method for a quasi-linear one-dimensional convection–diffusion problem, *SIAM J. Numer. Anal.* 39 (2001) 1446–1467.
- [7] N. Madden, M. Stynes, A uniformly convergent numerical method for a coupled system of two singularly perturbed linear reaction–diffusion problems, *IMA J. Numer. Anal.* 23 (2003) 627–644.
- [8] MATLAB R13 (Version 6.5), The MathWorks, Inc., www.mathworks.com.
- [9] H.-G. Roos, M. Stynes, L. Tobiska, *Numerical Methods for Singularly Perturbed Differential Equations: Convection–Diffusion and Flow Problems*, Springer Series in Computational Mathematics, vol. 24, Springer, Berlin, 1996.
- [10] A. Sandu, Positive numerical integration methods for chemical kinetic systems, *J. Comput. Phys.* 170 (2001) 589–602.
- [11] T.I. Seidman, L.V. Kalachev, A one-dimensional reaction/diffusion system with a fast reaction, *J. Math. Anal. Appl.* 209 (1997) 392–414.
- [12] L.F. Shampine, M.W. Reichelt, The MATLAB ODE suite, *SIAM J. Sci. Comput.* 18 (1997) 1–22.
- [13] A.M. Soane, M.K. Gobbert, T.I. Seidman, Design of an effective numerical method for a reaction–diffusion system with internal and transient layers, Technical Report-number 2006, Institute for Mathematics and its Applications, University of Minnesota, 2004.
- [14] M. Stynes, An adaptive uniformly convergent numerical method for a semilinear singular perturbation problem, *SIAM J. Numer. Anal.* 26 (1989) 442–455.
- [15] A.B. Vasil’eva, V.F. Butuzov, L.V. Kalachev, *The Boundary Function Method for Singular Perturbation Problems*, SIAM, Philadelphia, PA, 1995.